Check for updates

Aggregation induced emission based fluorenes as dual-channel fluorescent probes for rapid detection of cyanide: applications of smartphones and logic gates†

Shumaila Majeed,[a] Muhammad Tahir Waseem,[a] Hafiz Muhammad Junaid,[a] Gul Shahzada Khan,[b] Shamyla Nawazish,[c] Tariq Mahmood, [ID] [ab] Asad Muhammad Khan[a] and Sohail Anjum Shahzad [ID] *[a]

Rational modification of molecular structure by incorporating electron donating groups can play a potential role for designing aggregation induced emission (AIE) active fluorescent probes. Based on this principle, fluorescent probes (**1a–c**) were synthesized, and they displayed excellent aggregation induced emission (AIE) behavior in a H_2O/DMF (4 : 1, *v/v*) mixture due to restrictions in intramolecular charge transfer (ICT). As a comparison, probe **1d** was synthesized by installing an electron withdrawing ($-NO_2$) group that surprisingly quenched the aggregation behaviour. Additionally, AIE active probes **1a–c** displayed a highly sensitive dual channel (fluorometric and colorimetric) response towards rapid detection of CN^-, which is an active toxic material. Probes **1a–c** showed selectively enhanced fluorescence emission behavior towards CN^- with detection limits of 1.34 ppb, 1.38 ppb, and 1.54 ppb, respectively. The sensing mechanism involves Michael type adduct formation due to the nucleophilic addition reaction of cyanide with probes and was confirmed through ^1H NMR titration experiments. In contrast, probe **1d** containing an electron withdrawing moiety showed insensitivity towards CN^-. Therefore, this study provides the efficient strategy to induce AIE character in fluorescent probes and expands the mechanistic approach toward the sensing of toxic CN^-.

Introduction

The rational design and synthesis of aggregation-induced emission (AIE) active probes has acquired a lot of attention due to their broad range of applications such as fluorescence sensors[1] photodynamic therapy,[2] data security,[3] and organic light-emitting diodes (OLEDs).[4] However, many conventional fluorescent probes display high fluorescence emission in dilute solution, whereas the planarity, π–π stacking interaction, or excimers in solid or aggregated state quench their fluorescence emission. This phenomenon is known as aggregation-caused quenching (ACQ).[5] It markedly hampers the performance of fluorescent probes in high-tech applications because fluorescent probes are generally used in their solid/aggregated state for real-world applications. In contrast to ACQ, aggregation induced emission (AIE) active probes exhibit high fluorescence emission in the aggregated state and less or no emission in solution forms, which enormously increases their practical applicability.[6] Considering the extensive applicability, a large variety of AIE active fluorescent probes *viz.* tetraphenylethylene,[7] distyrylanthracene,[8] silole,[9] and carbazole derivatives[10] have been designed and synthesized depending upon different approaches. Previous studies proposed numerous mechanisms to decipher the AIE phenomenon such as restricted intramolecular rotation (RIR),[11] twisted intramolecular charge transfer (TICT),[12] intramolecular charge transfer (ICT),[13] and *cis–trans* isomerization.[14]

One effective strategy to induce AIE character is the installation of strong electron donor (D) moieties in fluorescent probes. In our recent approach aimed at construction of AIE active materials, it was intended to modify our previously reported fluorescent probe by incorporating strong electron donating groups in simple fluorene.[15] Interestingly, slight structural modifications (introduction of electron donors) in the attached moieties induced completely newer and unique feature of aggregation induced emission (AIE) due to electronic push–pull effect (Fig. 1). More importantly, this study extends the mechanistic approach that how an exquisite change in the

[a]Department of Chemistry, COMSATS University Islamabad, Abbottabad Campus, University Road, Abbottabad 22060, Pakistan. E-mail: sashahzad@cuiatd.edu.pk

[b]Department of Chemistry, College of Science, University of Bahrain, Sakhir 32038, Bahrain

[c]Department of Environmental Sciences, COMSATS University Islamabad, Abbottabad Campus, Abbottabad 22060, Pakistan

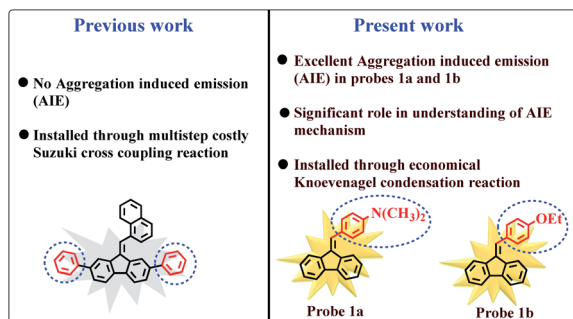† Electronic supplementary information (ESI) available. See https://doi.org/10.1039/d2ra03119a

Fig. 1 Structural comparison between our previously reported probe[15] and newly designed probes with new AIE properties.

molecular structure of fluorescent probe can modulate aggregation induced emission (AIE) properties. Further, it was noticed that the introduction of electron withdrawing group (–NO$_2$) in fluorene core (probe **1d**) quenched aggregation (ACQ) due to intersystem crossing. Therefore, this study brings a strategy to facilitate the development of efficient AIE active fluorescent probes.

Keeping in mind the broad applications of AIE active fluorescent probes, newly developed probes (**1a–d**) were efficiently used for the fluorescent detection of cyanide ions (CN$^-$), which is an active hazardous material. Long-term skin exposure of cyanide ions can lead to numerous health hazards, for example, hypoxia, loss of consciousness, endocrine disorders, convulsions, respiratory damage, and even death.[16] Up to present, various traditional detection methods *viz.* chromatography, voltammetry, potentiometry, and electrochemical methods have been developed for the efficient detection of toxic CN$^-$.[17–20] Yet, various disadvantages are associated with these traditional techniques *i.e.* complicated detection process, time-consuming, need bulky and expensive equipment that provides some room to exploit alternate appropriate detection methods. To compensate conventional methodologies, fluorescent probes are employed for the recognition and determination of targeted anions. They hold some promising predominance over the previous methodologies including high sensitivity, cost effective, facile operation, and efficient biological diagnosis.[21] At present, CN$^-$ probes have been categorized into different classes including hydrogen bonding,[22] nucleophilic addition,[23] coordination,[24] anion-metal affinity,[25] and deprotonation[26] depending upon their interaction with cyanide. Deprotonation and H-bonding based cyanide probes have quick response time but the detection process can easily be disturbed by other competing anions such as phosphate and fluoride. CN$^-$ probes based on coordination mechanism commonly involve two steps (*viz.* addition of metal ions and then adding cyanide) that make the recognition process quite inconvenient and tedious. On the other hand, nucleophilic addition reaction based CN$^-$ probes has anti-interference ability, sensitivity, and excellent selectivity due to the distinguished nucleophilic character of cyanide ions. In this context, olefin based fluorescent probes were designed and synthesized by Guo *et al.* for the detection of cyanide where CN$^-$ disturbed the conjugation system and thereby resulted in

the interruption of intramolecular charge transfer (ICT) process.[27] Cheng *et al.* synthesized indole based carboxycoumarin probe that underwent C=N nucleophilic addition reaction upon the attack of CN$^-$ to the indole unit.[28] However, aggregation caused quenching (ACQ) effect, slow response time, high detection limit, complicated synthetic procedures, and inefficiency of prior reported reaction based CN$^-$ probes in aqueous medium limit their applications in real environment.

In continuation of our efforts to design fluorescent probes,[6,15,29–38] newly synthesized probes (**1a–d**) offered valuable insight into the mechanistic approach involved in the sensing of CN$^-$. The introduction of –NO$_2$ substituted aromatic ring in probe **1d** seems to play decisive role, because electron withdrawing –NO$_2$ group did not allow the probe to bind or react with CN$^-$. Reduced reactivity of olefin functionality toward CN$^-$ may occur due to the presence of electron withdrawing –NO$_2$ group and formation of less stable carbocation. In fact, electron withdrawing groups make olefin moiety less favorable for nucleophilic addition reaction and *vice versa*. Sensing mechanism of nucleophilic addition reaction of probes and CN$^-$ was confirmed through ^{1}H NMR spectroscopy. The sensing ability of probes towards cyanide was further investigated through fluorescence emission, UV-visible absorption, computational studies, dynamic light scattering (DLS), and Jobs plots. To prove practicability, probes were utilized to detect CN$^-$ in easy to make test strips and for the detection of endogenous CN$^-$ ions in actual samples including peach kernel, bitter almond, and cassava.

Experimental

Synthetic procedure and characterization of compounds 1a, 1b, 1c, and 1d

9*H*-Fluorene (0.665 g, 4.0 mmol) was dissolved in 10.0 mL of ethanol followed by addition of potassium tertiary butoxide base (0.45 g, 4.0 mmol) and refluxed at 78 °C. After one hour, *N,N*-dimethylbenzaldehyde (1.46 mL, 12.0 mmol) was slowly added to the reaction mixture in an inert environment which resulted in orange-colored solution. The reaction mixture was further proceeded under reflux for 8 hours. Afterward, the reaction mixture was cooled to room temperature when fluorene was completely consumed. The desired compound was extracted with DCM and washed with brine and water twice in separating funnel. Anhydrous MgSO$_4$ was used as drying agent for the extracted organic layer. The solvent of organic layer was removed by using rotary evaporator. The crude solid material was further chromatographed by flash column chromatography using *n*-hexane/petroleum ether as eluent and compound **1a** was collected in orange-colored crystals. Yield: 74%; R_f = 0.70 (*n*-hexane); ^{1}H-NMR (400 MHz, CDCl$_3$) (δ ppm); 7.95 (d, J = 7.5 Hz, 1H, ArH), 7.77 (dd, J = 6.7, 1.7 Hz, 1H, ArH), 7.74–7.72 (m, 2H, ArH), 7.64 (s, 1H, olefinic CH), 7.56 (bd, J = 8.6 Hz, 2H, ArH), 7.36–7.28 (m, 3H, ArH), 7.12 (td, 1H, J = 7.8, 1.0 Hz, ArH), 6.80 (bs, 2H, ArH), 3.05 (s, 6H, N(CH$_3$)$_2$); ^{13}C (100 MHz, CDCl$_3$) (δ ppm); 141.0 (C), 140.2 (C), 138.8 (2 × C), 137.0 (C), 131.3 (2 × CH), 128.0 (C), 127.5 (C), 126.9 (CH), 126.6 (2 × CH), 124.1 (2 × CH), 120.0 (CH), 119.8 (CH), 119.6 (2 × CH), 112.2 (2 × CH),

40.8 (N(CH$_3$)$_2$). DEPT-135 NMR (100 MHz, CDCl$_3$) (δ ppm); 131.3 (2 × CH), 127.9 (CH), 127.4 (CH), 126.6 (2 × CH), 124.1 (2 × CH), 120.0 (CH), 119.8 (2 × CH), 119.6 (2 × CH), 43.8 (N(CH$_3$)), 40.6 (N(CH$_3$)).

The same procedure was opted to synthesize compounds **1b**, **1c**, and **1d** that resulted in the yellow, yellow, and grey colored crystals, respectively.

Compound **1b**; yield: 80%; R_f = 0.72 (*n*-hexane); ^{1}H-NMR (400 MHz, CDCl$_3$) (δ ppm); 7.77 (d, J = 7.2, 1H, ArH), 7.73 (d, J = 7.8, 3H, ArH), 7.65 (s, 1H, ArH), 7.54 (d, J = 8.5, 2H, ArH), 7.38–7.29 (m, 3H, ArH), 7.09 (t, J = 7.8, 1H, ArH), 6.97 (d, J = 8.6, 2H, ArH), 4.10 (q, J = 7.0, 2H, ArH), 1.47 (t, J = 6.7, 3H, CH$_3$). ^{13}C (100 MHz, CDCl$_3$) (δ ppm); 159.1 (C), 141.3 (C), 139.8 (C), 139.1 (C), 136.8 (C), 135.5 (C), 131.0 (2 × CH), 129.1 (CH), 128.4 (CH), 128.0 (CH), 127.6 (CH), 127.0 (CH), 126.7 (CH), 124.3 (CH), 120.2 (CH), 119.8 (CH), 119.6 (CH), 114.5 (2 × CH), 63.6 (CH$_2$), 15.0 (CH$_3$). DEPT-135 NMR (100 MHz, CDCl$_3$) (δ ppm); 131.0 (2 × CH), 128.4 (CH), 128.0 (CH), 127.6 (CH), 127.0 (CH), 126.7 (CH), 124.3 (CH), 120.2 (CH), 119.8 (CH), 119.6 (CH), 114.6 (2 × CH), 63.6 (CH$_2$), 15.0 (CH$_3$).

Compound **1c**; yield: 70%; R_f = 0.75 (*n*-hexane); ^{1}H-NMR (400 MHz, CDCl$_3$) (δ ppm); 7.76 (dd, J = 6.9, 1.1 Hz, 1H, ArH), 7.72–7.68 (m, 3H, ArH), 7.64 (s, 1H, olefinic CH), 7.55 (dd, 2H, J = 8.8, 0.6 Hz, ArH), 7.37–7.28 (m, 3H, ArH), 7.07 (dt, 1H, 7.6, 1.2 Hz, ArH), 6.97 (td, 2H, J = 5.4, 3.0 Hz, ArH), 3.88 (s, 3H, OCH$_3$); ^{13}C (100 MHz, CDCl$_3$) (δ ppm); 159.7 (C), 141.3 (C), 139.8 (C), 139.1 (C), 136.8 (C), 135.6 (C), 131.0 (2 × CH), 129.2 (C), 128.5 (CH), 128.1 (CH), 127.5 (CH), 127.1 (CH), 126.8 (CH), 124.3 (CH), 120.2 (CH), 119.9 (CH), 119.7 (CH), 114.1 (2 × CH), 55.5 (OCH$_3$). DEPT-135 NMR (100 MHz, CDCl$_3$) (δ ppm); 131.0 (2 × CH), 128.5 (CH), 128.1 (CH), 127.5 (CH), 127.1 (CH), 126.8 (CH), 124.3 (CH), 120.2 (CH), 119.9 (CH), 119.7 (CH), 114.1 (2 × CH), 55.5 (OCH$_3$).

Compound **1d**; yield: 69%; R_f = 0.74 (*n*-hexane); ^{1}H-NMR (400 MHz, CDCl$_3$) (δ ppm); 8.42 (s, 1H, ArH), 8.23 (dd, J = 8.2, 7.1, 1H, ArH), 7.90 (d, J = 7.6, 1H, ArH), 7.70 (d, J = 7.5, 1H, ArH), 7.69 (d, J = 7.1, 2H, ArH), 7.64–7.85 (m, 2H, ArH), 7.41–7.37 (m, 1H, ArH), 7.35–7.30 (m, 3H, ArH), 7.05–7.01 (m, 1H, olefinic H). ^{13}C (100 MHz, CDCl$_3$) (δ ppm); 148.6 (C), 141.8 (C), 139.6 (C), 139.0 (C), 138.8 (C), 138.7 (C), 135.9 (C), 135.5 (CH), 129.7 (CH), 129.4 (CH), 129.1 (CH), 127.4 (CH), 127.1 (CH), 124.3 (CH), 124.2 (CH), 123.7 (CH), 122.9 (CH), 120.6 (CH), 120.2 (CH), 119.9 (CH). DEPT-135 NMR (100 MHz, CDCl$_3$) (δ ppm); 135.5 (CH) 129.7 (CH), 129.4 (CH), 129.1 (CH), 127.4 (CH), 127.1 (CH), 124.3 (CH), 124.2 (CH), 123.7 (CH), 122.9 (CH), 120.6 (CH), 120.2 (CH), 119.9 (CH).

UV-visible and fluorescence experiments

1000 μM stock solutions of cyanide and all other anions (in the form of sodium salts) were prepared in H$_2$O/DMF (4 : 1, *v*/*v*). Targeted anions include CN$^-$, F$^-$, Cl$^-$, Br$^-$, I$^-$, ClO$_4$$^-$, N$_3$$^-$, NO$_3$$^-$, H$_2PO_4$$^-$, NO$_2$$^-$, and CH$_3COO^-$ ions. After optimizing the concentration with maximum emission, the UV-visible and fluorescence emission experiments of probes were performed without and with the gradual addition of anions ranging from 0 to 500 nM in ultimate 1000 μL H$_2$O/DMF (4 : 1, *v*/*v*) solution.

The quartz cuvette (path length, 10 × 10 mm; volume, 1000 μL) was utilized for fluorescence and UV-visible experimentation. The fluorescence experiments were performed at an excitation wavelength (λ_{exc}) of 340 nm opting slit width of 2/2 nm.

Calculation of fluorescence quantum yield

The fluorescence quantum yield (Φ) of probes (**1a–d**) was determined by using fluorescein as a standard compound (Φ = 0.95) at an excitation wavelength (λ_{exc}) of 340 nm and slit width of 2/2 nm on the spectrofluorophotometer. The quantum yields (Φ) of probes was calculated through eqn (1), where Φ_s and Φ_r represent the relative quantum yield of the samples and reference, respectively. A_s and A_r are equivalent to the absorbance of samples and reference, respectively. D_s is the area of emission of samples, while D_r is the area of emission of reference compound. The lengths of absorption cells is represented by L_s and L_r, whereas N_r and N_s are the refractive indices of the reference and sample solutions.

$$\Phi_s = \Phi_r \times (1 - 10^{-A_r L_r})/(1 - 10^{-A_s L_s}) \times N_s{}^2/N_r{}^2 \times D_s/D_r \quad (1)$$

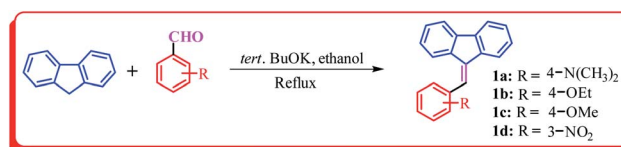Instruments and reagents used during this study are provided in the ESI (SI–1†).

Statistical data analysis

Fluorescence sensing experiments were presented as mean and standard deviation with n = 3. Statistical analysis of the obtained results was executed by employing GraphPad Prism with paired Student's *t*-test. Further, the linear fit model was evaluated through analysis of variance (ANOVA) (Table S1†); the value of $p < 0.05$ is statistically important. Similarly, normal data distribution (random error) and a confidence interval of 95% were considered for statistical evaluation.

Results and discussion

Synthesis and characterization

Fluorene based compounds **1a**, **1b**, **1c**, and **1d** were rationally synthesized from 9*H*-fluorene as shown in Scheme 1. Synthesis of compounds was accomplished in a single step. Compounds **1a**, **1b**, **1c**, and **1d** were developed through the Knoevenagel condensation reaction of 9*H*-fluorene with *N*,*N*-dimethylbenzaldehyde, 4-ethoxybenzaldehyde, 4-methoxybenzaldehyde, and 3-nitrobenzaldehyde, respectively by using potassium *tert*. butoxide as a base. The resulted compounds were characterized by ^{1}H, ^{13}C, and DEPT-135 NMR spectroscopy and are given in ESI (p. S19–S74†).

Scheme 1 Synthetic strategy to afford fluorene based compounds (**1a**, **1b**, **1c**, and **1d**) through the Knoevenagel condensation.

Effect of solvents

Since solvents' polarity may affect the ground and/or excited state energy levels and consequently shift the emission/absorbance of a probe to a lower/higher wavelength.[39] Hence, the fluorescence spectral properties of probes **1a**, **1b**, **1c**, and **1d** were evaluated in different solvents including ethyl acetate, tetrahydrofuran (THF), ethanol, methanol, acetonitrile (CH$_3$CN), dichloromethane (DCM), chloroform (CHCl$_3$), and toluene. Probes were insoluble in ethanol and methanol. Meanwhile, increasing solvents polarity from weakly polar toluene to strongly polar DMF, the fluorescence emission of probes **1a**, **1b**, **1c**, and **1d** was progressively red-shifted from 409, 410, 407, and 408 nm to 418, 414, 410, and 412 nm, respectively (Fig. S1†). The redshift in fluorescence emission was also associated with a considerable decrease in emission intensity. Conversely, the UV-visible absorption of probes **1a**, **1b**, **1c**, and **1d** at 370, 352, 353, and 300 nm displayed insignificant changes on varying the polarity of solvents (Fig. S1†). These spectral changes show that increase in solvents' polarity perturbs the intramolecular charge transfer (ICT) process, thereby affecting the fluorescence emission.

Aggregation induced emission (AIE) effect

Organic compounds are readily soluble in organic solvents but are commonly insoluble in water. Water insoluble compounds tend to agglomerate upon the addition of water that may subsequently alter the fluorescence emission. The possible changes in fluorescence emission of probes were investigated by using binary solvent system with varying water fractions from 0 to 90%. As shown in Fig. 2 and S2,† probes **1a** (20 μM), **1b** (50 μM), and **1c** (10 μM) were almost non-emissive in DMF. The fluorescence emission of probes was retained constant with a marginal decrease in emission along with a significant redshift until the water fraction reaches 30%. This is probably
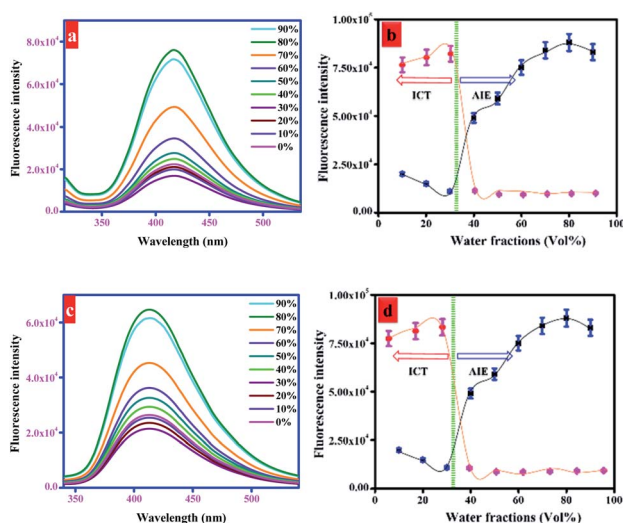
due to effective involvement of ICT process. Upon further addition of water fractions (f_w) from 30% to 80%, significant enhancement in fluorescence emission of probes **1a**, **1b**, and **1c** was noticed. It is due to the aggregate formation of probe molecules due to the addition of polar water that led to the restrictions in intramolecular rotations (IRs) and partially confined intramolecular charge transfer (ICT). It activates radiative decay process that ultimately results in enhanced fluorescence emission.[40] Meanwhile, when the water fraction increased from 80% to 90%, the fluorescence emission of probes slightly reduced that indicates the formation of amorphous aggregates at higher water contents (Fig. 2 and S2†). In contrary to this, the addition of water fractions (0–90%) considerably attenuated the fluorescence emission of probe **1d** (20 μM) (Fig. S2†). It shows that the introduction of nitro (–NO$_2$) group to **1d** led to the fluorescence quenching that is probably due to the internal conversion (IC) or intersystem crossing (ISC).[41] All these fluorescence changes are associated with color changes of probes (**1a–d**) under UV radiations (365 nm) upon gradual increase in water fractions in DMF solution. As
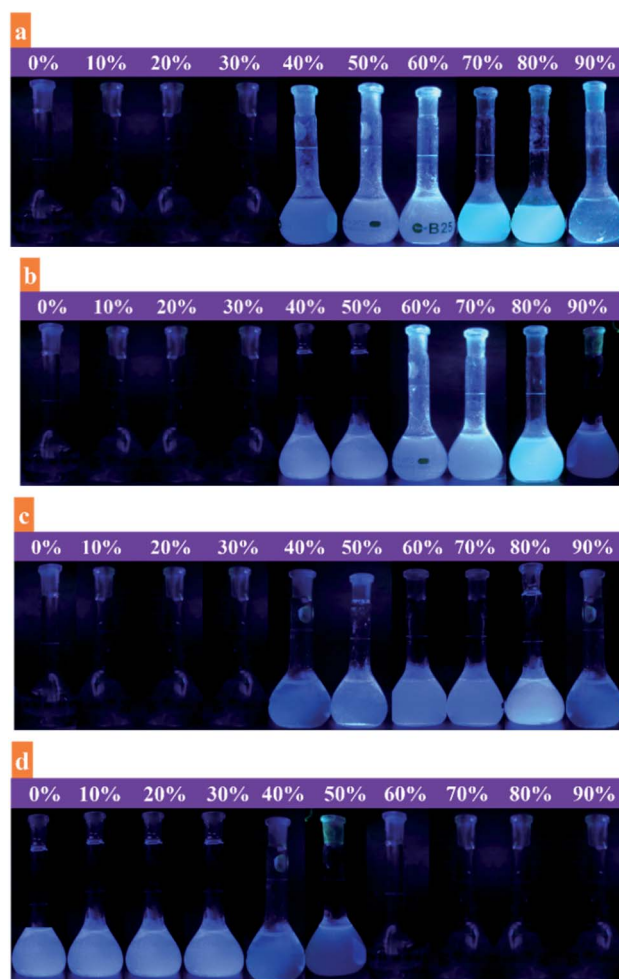

Fig. 2 Fluorescence spectra of probes **1a** (a) and **1b** (c) in DMF with increasing water contents from 0 to 90% (conc. = 20 μM (**1a**) and 50 μM (**1b**); λ_{ex} = 390 nm; slit width 2/2); general display of increase/decrease in fluorescence emission of probes **1a** (b) and **1b** (d) at different water fractions.

Fig. 3 The emission of probes **1a** (a), **1b** (b), **1c** (c) and **1c** (d) under UV radiations (365 nm) upon increasing water fractions (f_w = 0−90%) in DMF solutions (conc. = 20 μM (**1a**), 50 μM (**1b**), 10 μM (**1c**), and 20 μM (**1d**)).

evidenced in Fig. 3, the emission of probes (**1a–c**) was gradually increased up to 80% water and noticeably diminished upon the addition of water from 80 to 90%. However, fluorescence emission of probe **1d** was continuously reduced upon changing the water fractions from 0 to 90%. Next, the fluorescence quantum yield of probes (**1a–d**) was measured by using eqn (1) (given in experimental part) to further decipher the aggregation induced emission (AIE) character. The quantum yields (Φ) of probes **1a**, **1b**, **1c**, and **1d** were calculated as 0.23, 0.28, 0.35, and 0.59, respectively in DMF. The quantum yields (Φ) of probes **1a**, **1b**, and **1c** were substantially increased to 0.67, 0.63, and 0.58 in H_2O/DMF mixture with 80% water fractions (f_w). However, probe **1d** observed a notable decrease in quantum yield to 0.25. These outcomes support the strong emissive behavior of probes **1a**, **1b**, and **1c** in aggregated state.

Further, the fluorescence emission of probes (**1a–c**) was investigated in ethylene glycol/DMF mixture with different ethylene glycol fractions (f_w). It was assumed that the fluorescence emission of probes would be substantially enhanced upon the addition of more viscous solvent, ethylene glycol. It is demonstrated in Fig. S3† that the emissions of probes **1a**, **1b**, and **1c** showed distinct response in ethylene glycol/DMF mixture (ethylene glycol; 0–90%), suggesting the aggregate formation as a reason for their enhanced fluorescence emissions. This splendid fluorescence emission enhancement was quantified by establishing a linear fit plot taking fluorescence intensity as a function of ethylene glycol fractions (Fig. S3†). Additionally, the aggregation induced emission (AIE) behavior was justified through the concentration dependent fluorescence emission response of probes (**1a–c**) in H_2O/DMF (4 : 1, v/v). Upon increasing the concentrations of probes from 0 to 50 μM, probes **1a**, **1b**, and **1c** displayed very weak fluorescence emissions with marginal better emission at 20 μM, 50 μM, and 10 μM (Fig. S4†) concentrations. These results evidently favor that fluorescence emission of probes is enhanced due to aggregate formation (AIE) and not because of concentration changes.

Sensing studies

pH effect. Occasionally, small changes in pH influence the fluorescence response of probes towards anions. To check the applicability of probes, fluorescence spectra of probes were recorded in H_2O/DMF (4 : 1, v/v) system before and after the addition of CN^- (500 nM) over a wide pH range (2.0–12.0). Fig. S5† implies the enhanced fluorescence response of probes towards CN^- in the pH range of 7.5–8.5. However, probes displayed insignificant fluorescence response in the acidic pH (0–6.5 pH) which shows that probes didn't undergo a nucleophilic addition reaction with CN^- in an acidic medium. Furthermore, study of pH effect articulates that probes are ideal to detect CN^- in aqueous medium with a rapid response time since the addition of excess amount of NaCN in water changes its pH from 7.0 to 8.3–8.5 that relates the optimized pH of probes.

Absorption studies

Probes possess characteristic vinyl functionality installed at C-9 position, at which a substrate with excellent nucleophilic character can favorably react that may tune up their photophysical properties. Keeping this in mind, the sensing potential of probes **1a** (20 μM), **1b** (50 μM), **1c** (10 μM), and **1d** (20 μM) towards various anions used in the form of sodium salts CN^-, F^-, Cl^-, Br^-, I^-, ClO_4^-, N_3^-, NO_3^-, $H_2PO_4^-$, NO_2^-, and CH_3COO^- (500 nM) was investigated in H_2O/DMF (4 : 1, v/v). On determining through UV-visible absorption spectrophotometer, probes alone (**1a**, **1b**, **1c**, and **1d**) displayed an intense
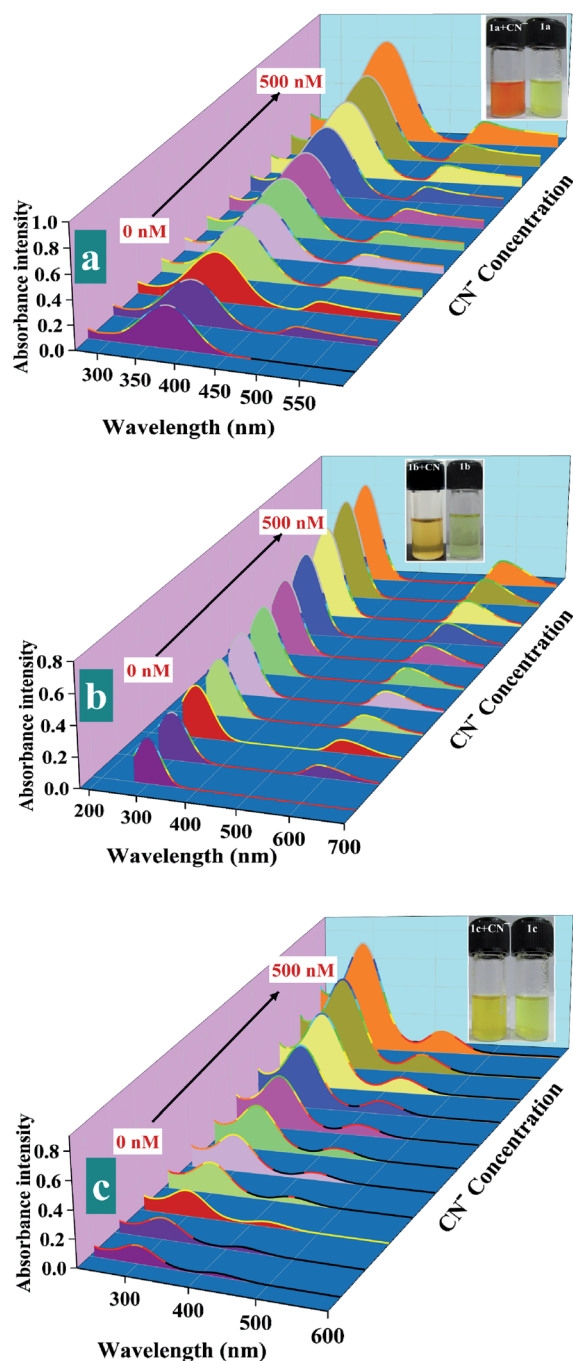

Fig. 4 Absorption spectra of probes **1a** (a), **1b** (b) and **1c** (c) upon the addition of 0−500 nM of CN^- (conc. = 20 μM of (**1a**) and 50 μM of (**1b**), and 10 μM (**1c**)); insets display naked eye color change upon the addition of only CN^- (1 μM).

characteristic band at 370, 352, 353, and 300 nm, respectively. Upon the addition of CN⁻, the intensity of (**1a**, **1b**, and **1c**) characteristic peaks was increased and a completely new sharp peak appeared at 505, 590, and 425 nm (Fig. S6†). However, other anions were unable to perturb the absorption of probes. Interestingly, probe **1d** remained insensitive towards all targeted anions. These experimental findings clearly indicate that probes are highly selective towards the detection of CN⁻ except probe **1d** that remained insensitive towards targeted anions. Selective detection of CN⁻ is probably ascribed to its greater nucleophilicity, strong basicity, weak hydration enthalpy (−295 kJ mol⁻¹) in semi-aqueous medium as compared to other anions.[42] However, the inability of probe **1d** to sense CN⁻ is probably due to its electron withdrawing group (–NO₂) that didn't favor the nucleophilic reaction to occur.

Next, the sensitivity of probes **1a** (20 μM), **1b** (50 μM), **1c** (10 μM) towards CN⁻ was elaborated through UV-visible titration of probes by adding incremental concentration of CN⁻. As the concentration of cyanide was increased from 0 to 500 nM, gradual hyperchromic shift in the characteristic UV-visible absorption band of probes was noticed along with an appearance of a completely new band at 505, 590, and 425 nm that denotes the formation of new species (Fig. 4). Besides, obvious color change of probes **1a**, **1b**, and **1c** from yellow, greenish, and light yellow to dark red, brown, and bright yellow during the titration experiment also favors the formation of new species (Fig. 4; insets).

Following the absorption experiments, a linear calibration curve was plotted for each of the probes **1a**, **1b**, and **1c** to exclusively quantify the direct relation between the gradual increases in the CN⁻ ions concentration (0–500 nM) and elevation in the absorption intensity (Fig. S7†).

Fluorescence emission study

To evaluate the sensing potential of probes toward CN⁻, the fluorescence emission studies of probes **1a** (20 μM), **1b** (50 μM), **1c** (10 μM), and **1d** (20 μM) were carried out in H_2O/DMF (4 : 1, v/v) without and with the addition of targeted anions *viz.* CN⁻, F⁻, Cl⁻, Br⁻, I⁻, ClO_4^-, N_3^-, NO_3^-, $H_2PO_4^-$, NO_2^-, and CH_3COO^-. It is evident in Fig. S8† that the concomitant addition of different anions, except CN⁻, didn't change the fluorescence emission of probes **1a**, **1b**, and **1c**, respectively. With the addition of CN⁻, the fluorescence emission intensity of probes **1a**, **1b**, and **1c** was abruptly increased with an observable redshift of 13, 8, and 5 nm, respectively. The selective fluorometric response of probes toward CN⁻ is probably due to the disruption in π conjugation of probes upon the addition of CN⁻ ions.[43] As expected, the fluorescence emission of probe **1d** at 412 nm was retained unaltered upon the addition of targeted anions (Fig. S8†). These results substantiated the excellent selectivity of probes **1a**, **1b**, and **1c** towards CN⁻. In addition, effect of potential interferences was also investigated by simultaneous addition of targeted anions (20 equiv.) to the H_2O/DMF (4 : 1, v/v) solution of probes containing CN⁻ (500 nM). As evidenced from the results presented in Fig. S9,† fluorescence enhancement efficiencies of probes **1a** (34 folds), **1b** (27 folds), and **1c**

(21 folds) against CN⁻ ions were not affected in the presence of other interferences, signifying favored selectivity of probes toward CN⁻ even in complex environment.

To elaborate the fluorescence sensing potential of probes, the fluorescence titration experiments were performed by the
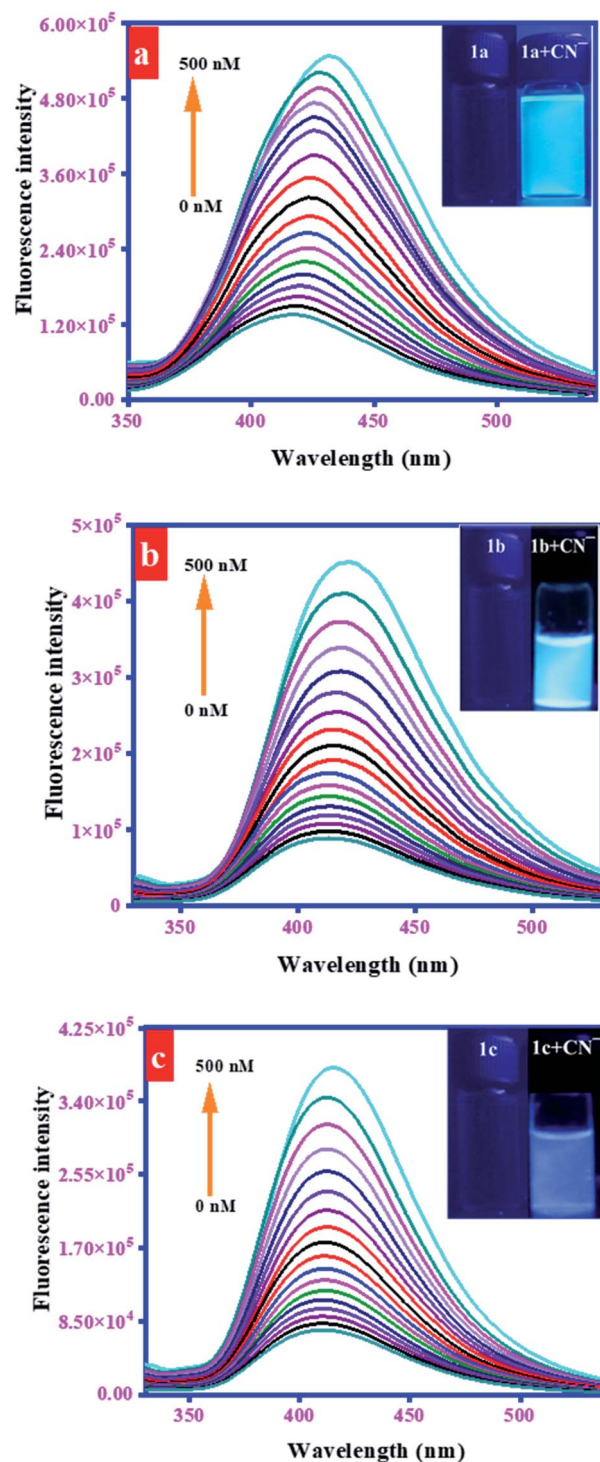

Fig. 5 Fluorescence spectra of probes **1a** (a), **1b** (b), and **1c** (c) upon the addition of 0–500 nM of CN⁻ (conc. = 20 μM (**1a**), 50 μM (**1b**), and 10 μM (**1c**); λ_{ex} = 390 nm; slit width 2/2); insets display naked eye color change upon the addition of only CN⁻ (1 μM).

progressive addition of CN⁻ (0–500 nM) to H₂O/DMF (4 : 1, *v*/*v*) solution of probes **1a** (20 μM), **1b** (50 μM), and **1c** (10 μM). As a result, the fluorescence emission of probes centered at 418, 414, and 410 nm was gradually increased with a concomitant redshift to 431, 422, and 415 nm, respectively (Fig. 5). A linear correlation was observed between relative fluorescence intensity (F/F_0) and CN⁻ concentrations in the range of 0–500 nM. This response was justified through linear calibration curves, correlation coefficient along with regression equation, provided in these curves (Fig. S10†). The precision in the fluorescence determination of the CN⁻ ions was evaluated through relative standard deviation (RSD) (eqn (2)). It was calculated after three replicate determinations (0–500 nM) of the CN⁻ ions and was calculated to be 1.44%.

$$\text{RSD} = (s_p/x_p) \times 100 \qquad (2)$$

where s_p represents the standard deviation, and x_p denotes the average of a given analytical standard ($n = 3$). Further, these spectral changes were accompanied by the appearance of bright emission of probes under UV radiations (365 nm) upon the addition of CN⁻ (1 μM) (Fig. 5; insets). The binding constant (K_a) for the reaction of probes with CN⁻ was calculated through fluorescence titration experiments using the Benesi–Hildebrand equation. Plots of relative increase in fluorescence emission of probes with increasing concentrations of CN⁻ displayed excellent linear behavior and estimated binding constant values were determined to be 2.23×10^6 M⁻¹ (**1a**), 1.0×10^6 M⁻¹ (**2a**), and 3.42×10^5 M⁻¹ (**3a**) (Fig. S11†).

The high magnitude of the binding (association) constants (K_a) implied a strong association between probes and CN⁻. Moreover, the binding stoichiometry between probes and CN⁻ was studied through the continuous variance method (Job's plot). For this purpose, equimolar solutions (50 μM) of probes and CN⁻ were prepared and Job's plots were made between relative fluorescence emission and increasing mole fractions of CN⁻. The resulting plots given in Fig. S12† show the highest intensity at the composition of 0.5 : 0.5 of probes–CN⁻ complex confirming the 1 : 1 binding stoichiometry and excellent sensitivity of probes with CN⁻. Distinguished sensitivity of probes for the sensing of CN⁻ was further estimated through their limits of detection (LOD). The LODs of probes were determined through the IUPAC recommended protocols, using formula LOD = $3\sigma/S$, where σ is the standard deviation and S corresponds to the slope of the plot between fluorescence intensity of probes *versus* cyanide concentration. The calculated detection limits of probes **1a**, **1b**, and **1c** for the detection of CN⁻ were found out as 1.34 ppb, 1.38 ppb, and 1.54 ppb, respectively. These values are sufficiently lower than the WHO limit of CN⁻ concentration in aqueous medium (1.9 μM).[44] Calculated LOD values are based on the standard deviation from the blank signal intensity of the probes in triplicate experiments.

Sensing mechanism

¹H NMR titration study. ¹H NMR titration study of probe **1a** without and with the addition of cyanide (in the form of NaCN)
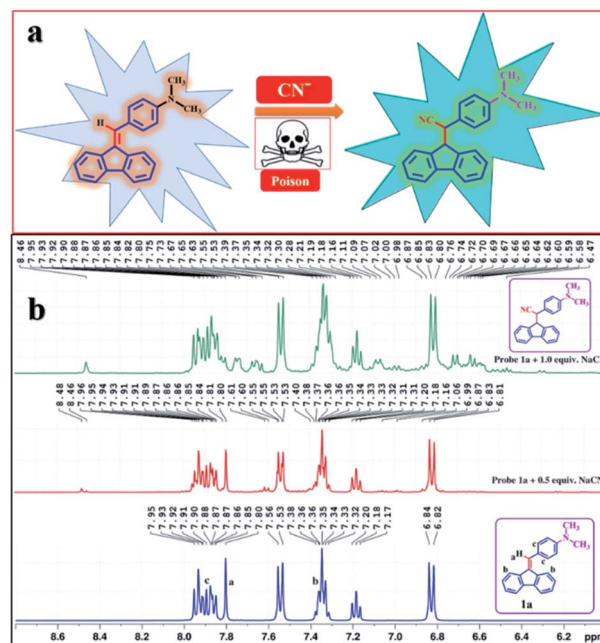

Fig. 6 (a) Plausible reaction mechanism between AIE active probe **1a** and CN⁻; (b) ¹H-NMR titration spectra of probe **1a** before and after the addition of 0–1.0 equiv. of CN⁻ in DMSO-d_6.

was carried out in DMSO-d_6 to delineate the sensing mechanism for the detection of CN⁻. As shown in Fig. 6, alone probe **1a** displayed three signals appeared at δ 7.80, 7.38–7.32, and 7.87–7.85 ppm corresponding to vinyl proton (H_a), two aromatic protons present in fluorene core (H_b), and two aromatic protons present in attached phenyl unit (H_c). Upon successive addition of CN⁻ (0–1.0 equiv.), vinyl proton peak was disappeared and all aromatic protons were shifted completely upfield. All these spectral changes are evidence of covalent interaction between probe and CN⁻ that resulted in the formation of a new Michael type adduct. However, to obtain the covalent interaction, the probe–CN⁻ mixture was kept for 1 hour after mixing the each equiv. (0.5 and 1.0) of CN⁻ to probe.

The sp²-hybridized vinyl carbon of probe **1a** (**1b**, **1c**, and **1d**) renders alkene carbon slightly electrophilic/carbocation. Electrophilic carbon (partially carbocation) is stabilized by conjugation with electron donating groups (in **1a**, **1b**, and **1c**). As a result, stabilized vinyl carbon undergoes nucleophilic addition reaction with a strong nucleophile, CN⁻ that consequently generates Michael type adduct as illustrated in Fig. 6. On the other side, electron withdrawing group (–NO₂) attached to probe **1d** makes its vinyl carbon less stable and less favorable for nucleophilic addition reaction initiated by CN⁻. Fluorescence results clearly show that probes **1a**, **1b**, and **1c** favorably react with CN⁻ but probe **1d** remained completely insensitive towards CN⁻.

Density functional theory (DFT) study. The sensing CN⁻ was further substantiated through FMOs analysis *via* density functional theory (DFT) calculations by using Gaussian 09 software,[45] at B3LYP/6-31G (d) method.[46,47] FMOs analysis is very useful for analyzing the change in electronic properties before
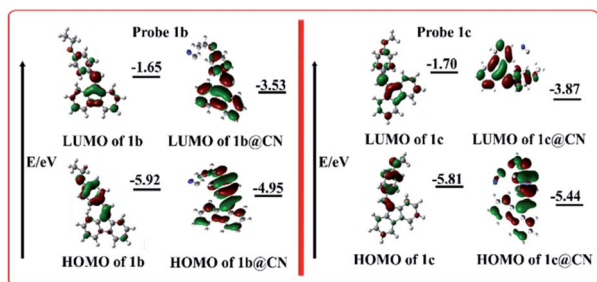
Fig. 7 The HOMO–LUMO energy level diagram for probes **1b** and **1c** and their CN⁻ complexes.

and after the complexation of probes.[48–50] FMOs plots of probes and their corresponding CN⁻ complexes are given in Fig. 7 and S13.† As evident from Fig. 7 and S13,† the highest occupied molecular orbitals (HOMOs), in isolated probes, are mainly located on the attached aromatic moieties and vinyl position and the lowest unoccupied molecular orbitals (LUMO) are distributed over fluorene units. Such dispersion of molecular orbitals (MOs) accounts for the intramolecular charge transfer (ICT) process. However, HOMO/LUMOs distribution differs after sensing of CN⁻ at vinyl position, which demonstrates the disturbance in ICT transition and is responsible for changes in photophysical properties. Moreover, reduction in the HOMO–LUMO (H–L gap) energy gap of probes **1a** (4.32 eV), **1b** (4.27 eV), and **1c** (4.11 eV) to 1.22 eV (**1a**–CN⁻), 1.42 eV (**1b**–CN⁻), and 1.57 eV (**1c**–CN⁻) proves the formation of very stable probe–CN⁻ adduct.

Dynamic light scattering (DLS) study. Formation of probe–CN⁻ adduct was further supported by the dynamic light scattering (DLS) measurements. As shown in Fig. S14,† the average particle size of probes **1a** (20 μM) and **1b** (50 μM), (as a model) in H₂O/DMF (4 : 1, v/v) was estimated as 142 (PDI: 0.531) and 220 nm (PDI: 0.534), respectively.

Stability test and response time study. Upon concomitant addition of CN⁻ (500 nM), particle size of probes was significantly reduced to 9.1 nm (**1a**–CN⁻, PDI: 0.331) and 164 nm (**1b**–CN⁻, PDI: 0.334). Reduction in particle size is clear evidence of disturbance in ICT transitions and new de-aggregated adduct formation that consequently resulted in the enhanced fluorescence emission.[51]

Practical applicability of a probe can be evaluated through its photostability and quick response time. To estimate extent of photostability, probes (**1a**, **1b**, and **1c**) and probe–CN⁻ adducts were subjected to high energy excited radiations and their fluorescence emission spectra were recorded after regular intervals of time (10–100 s). Results given in Fig. S15† disclose that fluorescence emission of probes and probe–CN⁻ adducts was not affected by their continuous exposure to high energy radiations that substantiate their photostability. Additionally, emission enhancement response of probes was studied in H₂O/DMF (4 : 1, v/v) as a function of time (0–60 s) after the addition of CN⁻ (500 nM).

It was noticed that probes **1a**, **1b**, and **1c** displayed significant fluorescence enhancement behavior after 20, 25, and 35 s

of cyanide addition that ensures their quick response time towards sensing of CN⁻ (Fig. S16†).

Practical applications

Solid-supported detection of CN⁻. During the past few years, solid-state emitting materials have attracted a lot of attention in the domain of fluorescence sensors and organic light emitting diodes (OLEDs).[52] An enhanced emission in solid-state is a prerequisite for the fabrication of devices to be used in organic electronics applications (*i.e.* OLEDs). Strong fluorescence enhancement response of probes **1a**, **1b**, and **1c** to CN⁻ in solution stimulated us to develop an effective solid-supported emitters for the useful detection of CN⁻. Moreover, development of solid-supported detection tool greatly enhances the portability of sensing process and effectively reduces the detection cost. In this context, cyanide responsive test strips were prepared by immersing thin layer chromatographic (TLC) plates (300 μm) into THF solution of probes **1a** (20 μM), **1b** (50 μM), and **1c** (10 μM) and air dried. Probe coated test strips were dipped in THF solution of CN⁻ and other targeted anions (500 nM) and dried in the oven at 30 °C for 20 min. Out of these test strips, the one dipped in CN⁻ solution alone displayed strong fluorescence emission under UV radiations (365 nm) and all other test strips were non-responsive to other treated anions as shown in Fig. 8 and S17.† These observations clearly indicate that newly developed probes' coated test strips can potentially be applied for instant colorimetric identification of CN⁻ ions. The similar probes' coated test strips were used to detect CN⁻ ions after regular intervals of 30 and 60 minutes (Fig. S18†). The results were comparable to previous observations. This demonstrates the detection accuracy and storage stability of the probes on test strips.

Detection of CN⁻ in industrial waste. Cyanide liberates from pharmaceutical waste materials and form hydrogen cyanide (HCN) in air that is known to cause cyanide toxicity in nearby areas. Prolonged inhalation in HCN saturated area can cause nerve damage that may lead to the human death.[53] Hence, it is highly dispensable to sense cyanide in industrial wastewater in order to avoid cyanide toxicity. Accordingly, probe **1a** was applied to recognize CN⁻ in pharmaceutical wastewater (collected from Islamabad Pharma Abbottabad, Pakistan). For this purpose, collected wastewater samples were filtered to remove inessential particles followed by spiking different concentrations of CN⁻ (200 and 500 nM). Prepared water samples were added to H₂O/DMF (4 : 1, v/v) solution of probe **1a** (20 μM) and fluorescence emission spectra were recorded under already optimized parameters. Obtained results revealed that
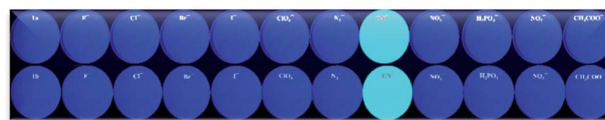

Fig. 8 Color change of probes' **1a** and **1b** coated test strips upon dipping in THF solution of CN⁻ and other anions (500 nM).

Table 1 Recovery of CN⁻ spiked in industrial wastewater by probe **1a**

Sr. No.	Spiked (nM)	Recovered (nM) (mean ± SD)	Recovery (%)	RSD (%) ($n = 3$)
1	0	0	—	—
2	200 nM	198 ± 0.02	98	2.08
3	500 nM	504 ± 0.01	102	1.07

addition of cyanide containing waste water resulted in significant fluorescence emission enhancement (Fig. S19†). Fluorescence enhancement results were compared with fluorescence response of probe towards laboratory sample to quantify CN⁻ ions. Experimental outcomes given in Table 1 provided cyanide recovery more than 97% with <2.1 RSD that ensure the practical applicability of probes presented in this study. These experiments further justify the accuracy and stability of the method.

Detection of endogenous CN⁻ in food samples. The accuracy of the method was validated by determining the CN⁻ ions concentration in food samples. It is well known that peach kernel and bitter almonds have high medicinal significance. However, endogenous enzymes have tendency to break cyanoside into hydrogen cyanide (HCN), if these kernels are not properly processed.[54] Similarly, cassava is appetizing because high starch is found in its rhizome. However, in unfavorable temperature and humid environment, cyanogenic glycosides undergo enzymatic hydrolysis to release hydrocyanic acid (HCN). HCN, consequently, can cause cyanide poisoning in human and animals.[54] Hence, it is important to detect endogenous cyanide in these food materials. To attain this object, peach kernel, bitter almond, and cassava powder (20 g) were mixed with 1.0 g NaOH and mixtures were subjected to sonication for 30 min at 25 °C followed by filtration to eradicate undesired suspended particles.

Upon addition of peach kernel, bitter almond, and cassava powder containing solution to the H₂O/DMF (4 : 1, v/v) solution of probes **1a** (20 μM), **1b** (50 μM), and **1c** (10 μM), fluorescence emission of probes was significantly enhanced as shown in Fig. 9 and S20.† Further, developed probes' coated test strips also displayed significant fluorescence emission under UV radiations (365 nm), when a single drop of these solutions was applied (Fig. 9 and S20;† insets). These results revealed that probes can be used for recognition of endogenous cyanide in food materials. Further, to validate the accuracy of the adopted method, a range of CN⁻ concentrations (100–500 nM) was spiked in cassava samples and fluorescence spectra were recorded. Afterward, a calibration curve was plotted that represents the direct co-relation between CN⁻ concentration and enhanced fluorescence emission (Fig. S21†). These results justify the accuracy and stability of the adopted method.

Construction of logic gate. In recent past, fabrication of logic devices based on variations in fluorescence signals into chemically encrypted information has drawn attention in the field of an unconventional computing system.[60] Therefore, an obvious redshift in fluorescence emission of probe **1a** (418–431 nm) upon the addition of CN⁻ (500 nM) impetus us to design logic gates. In this regard, AND, OR, NOT, and XOR gates were
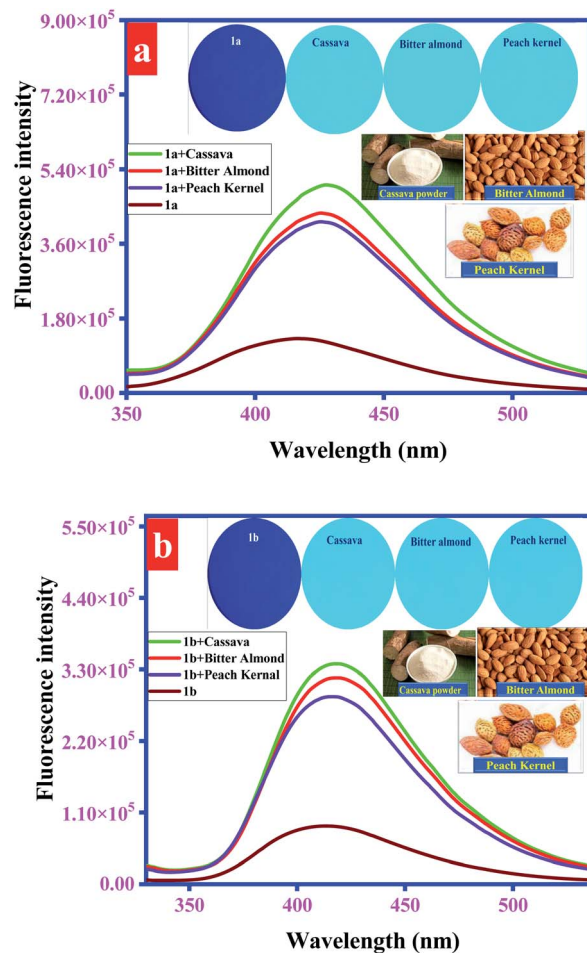

Fig. 9 Fluorescence spectra of probes **1a** (a) and **1b** (b) upon the addition of H₂O/DMF (4 : 1, v/v) solution of peach kernel, bitter almond, and cassava powder (conc. = 20 μM (**1a**), 50 μM (**1b**) and 10 μM (**1c**); λ_{ex} = 390 nm; slit width 2/2).

utilized to construct a logic circuit in which probe **1a** lone and **1a**–CN⁻ adduct were considered as input-1 (In-1) and input-2 (In-2), respectively. Fluorescence emission at 431 nm was used as an output (OUT) signal (Fig. 10). Fluorescence wavelength of 431 nm was arbitrarily selected as threshold limit and output (OUT, emission wavelength) lower than threshold limit (431 nm) is designated as "0" or "OFF" state whereas equal or larger than the threshold limit is considered as "1" or "ON" state. As it is evident in Fig. 10, only when **1a**–CN⁻ adduct (In-2) is present (0,1)/(1,1), output (OUT) at 431 nm is on "1" or "ON" state of the
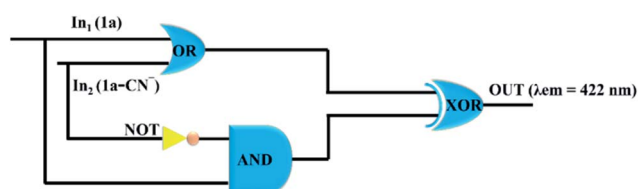

Fig. 10 Representation of logic gate designed through the fluorescence response of probe **1a** upon the addition of CN⁻.

Table 2 Truth table for logic circuit

In-1 (1a alone)	In-2 (1a–CN⁻)	OUT (λ_{em} = 431 nm)
0	0	0
0	1	1
1	0	0
1	1	1

system. Other variations such as when both **1a** lone (In-1) and **1a**–CN⁻ (In-2) or only **1a** lone are absent, the output (OUT) signal at 418 nm is lower than threshold limit and exhibits "0'' or "OFF" state. These variations are summarized in truth table (Table 2).
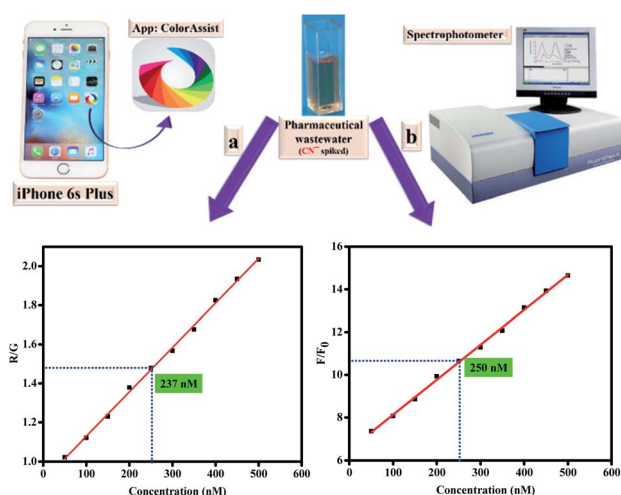

Fig. 11 (a) Smartphone-assisted RGB (Red, Green, and Blue) responses for the determination of CN⁻; (b) fluorescence spectral response for the determination of CN⁻.

Smartphone APP based detection of CN⁻. In the present era, usage and availability of smartphones have tremendously increased around the globe. Smartphones have revolutionized the world in terms of offering excellent computing power, in-built sensors, and high-resolution coverage. These features drawn our attention towards quick quantitative detection of CN⁻ in laboratory and real samples. As discussed earlier, probe **1a** displayed sharp color change from yellow to dark red upon the addition of CN⁻. Herein, smartphone APP was used for convenient detection of CN⁻ based on RGB (Red, Green, and Blue) color scale. On RGB color scale, each color is indicated by a specific whole number in between 0 and 255. For example, the number scale [0,0,0] corresponds to absolute black while [255,255,255] is attributed to the true white. Using a smartphone (model: Apple iPhone 6s Plus), color assist (freely available APP) was used to record variations in RGB (Red, Green, and Blue) values when naked eye color change was noticed upon the progressive addition of CN⁻ (0–500 nM) to the H₂O/DMF (4 : 1, v/v) solution of probe **1a**. Subsequently, a plot was produced between the ratio of red and green (R/G) and increasing concentrations of CN⁻ that displayed excellent linear response (R^2 = 0.97923) and limit of detection (LOD) was found out as 13.7 nM (Fig. 11).

To substantiate the validity of the method, pharmaceutical wastewater containing specific concentration of CN⁻ was tested quantitatively through color assist APP and fluorescence spectrophotometer independently. After comparison of obtained results with laboratory samples, the concentration of CN⁻ spiked in wastewater was determined as 237 nM through smartphone APP. Besides, concentration determined through fluorescence enhancement response was 250 nM (Fig. 11). It revealed that smartphone APP based determination of CN⁻ in real samples provided excellent results with 95% accuracy. These results provide portable, low cost and convenient approach in terms of probes (presented in this study) for the qualitative and quantitative detection of CN⁻.

Table 3 Comparison of probe **1a** with already reported cyanide responsive probes

Sensors type	Fluorescence response	Applications	LOD	Ref.
Fluorene based probe **1a**	Fluorescence emission enhancement	Smartphone based detection, logic gate, test strips, industrial and food samples	1.34 ppb (27.3 nM)	Present study
Rhodamine based fluorophore	Fluorescence emission enhancement	Cyanide detection in tap water	0.81 μM	55
Azobenzene based fluorometric and colorimetric sensor	Fluorescence emission enhancement	Test strip	1.1 μM	56
Azomethine sensor for detection of cyanide in aqueous medium	Fluorescence emission enhancement	Test strip	1.03 μM	57
Pyrene based cyanide sensor	Fluorescence emission enhancement	Test strip	1.98 μM	17
Triphenylamine (TPA) based probes	Fluorescence emission enhancement	Hela cell imaging	234 nM	58
Phenanthroimidazole and dicyanovinyl functionalized probes	Fluorescence emission enhancement	Paper strip and real water samples	0.23 μM	59

Comparison study. The fluorescence sensing potential of probes towards cyanide was compared with CN^- probes reported in literature and summarized in Table 3. Summarized data reveal that probes reported in this study are much better, exhibiting distinguished sensitive response towards CN^- in a wide pH range and with a very low detection limit. Facile synthesis, aggregation induced emission (AIE) character, broad range of practicability, and dual channel sensing (fluorescent and colorimetric) in semi–aqueous medium provides them an additional advantage in comparison to prior reported CN^- sensors.

Conclusions

In summary, four new simple fluorene based fluorescent probes were synthesized through a single step Knoevenagel condensation reaction that displayed strong aggregation induced emission (AIE) behavior. AIE character was accomplished due to the restriction in intramolecular charge transfer (ICT). Further, aggregation caused quenching (ACQ) character exhibited by probe **1d** (with no ICT) favors the restriction in intramolecular charge transfer (ICT) as a key factor for AIE. Additionally, AIE active probes displayed fluorescence emission enhancement response towards the recognition of cyanide that was ascribed to the Michael type adduct formation. Cyanide reacts at vinyl position of probes that results in the disturbance of intramolecular charge transfer process, thereby causing enhanced fluorescence response. Nucleophilic addition reaction was confirmed through NMR titration experiments, theoretical and DLS studies. Besides, probes exhibited selective colorimetric detection of CN^- that was readout through smartphone assisted application. Moreover, enhanced fluorescence response of probes for CN^- was exploited to design logic circuit. Advantageously, simple fluorescent probes were able to sense CN^- in food materials, industrial samples and through cyanide responsive test strips. Conclusively, this study facilitates to understand structure–property relationship and provides an extended mechanistic approach for the sensing of CN^-.

Author contributions

Shumaila Majeed: conceptualization, visualization, methodology, investigation, software, validation, formal analysis, writing – original draft. **Muhammad Tahir Waseem**: methodology, conceptualization, formal analysis, writing – original draft. **Hafiz Muhammad Junaid**: visualization, software, validation, formal analysis. **Gul Shahzada Khan**: investigation, methodology, resources. **Shamyla Nawazish**: validation, formal analysis. **Tariq Mahmood**: data curation, software, formal analysis. **Asad Muhammad Khan**: validation, formal analysis. **Sohail Anjum Shahzad**: supervision, conceptualization, methodology, visualization, validation, investigation, project administration, funding acquisition, writing – review & editing.

Conflicts of interest

The authors declare no conflict of interest.

Acknowledgements

Notes and references

1 M. Yuan, X. Fang, Y. Wu, Y. Xu, H. Feng, J. Mu, Z. Chen, Y. Lin, Q. Fu and W. Du, Activatable nanoprobe with aggregation-induced dual fluorescence and photoacoustic signal enhancement for tumor precision imaging and radiotherapy, *Anal. Chem.*, 2022, **94**(12), 5204–5211, DOI: **10.1021/acs.analchem.2c00340**.

2 X. Min, F. Yi, X.-L. Han, M. Li, Q. Gao, X. Liang, Z. Chen, Y. Sun and Y. Liu, Targeted photodynamic therapy using a water-soluble aggregation-Induced emission photosensitizer activated by an acidic tumor microenvironment, *Chem. Eng. Sci.*, 2022, **432**, 134327, DOI: **10.1016/j.cej.2021.134327**.

3 V. J. Kumar, J.-Z. Wu, M. Judd, E. Rousset, M. Korb, S. A. Moggach, N. Cox and P. J. Low, The syntheses, structures and spectroelectrochemical properties of 6-oxoverdazyl derivatives bearing surface anchoring groups, *J. Mater. Chem. C*, 2022, **10**, 1896–1915, DOI: **10.1039/D1TC05495C**.

4 L. Stojanović and R. Crespo-Otero, Emission quenching in tetraphenylfuran crystal: Why this propeller-shaped molecule does not emit in the condensed phase?, *Molecules*, 2022, **27**, 522, DOI: **10.3390/molecules27020522**.

5 S. Hussain, H. M. Junaid, M. T. Waseem, W. Rauf, A. J. Shaikh and S. A. Shahzad, Aggregation-induced emission of quinoline based fluorescent and colorimetric sensors for rapid detection of Fe^{3+} and 4-nitrophenol in aqueous medium, *Spectrochim. Acta, Part A*, 2022, **272**, 121021, DOI: **10.1016/j.saa.2022.121021**.

6 S. Hanif, H. M. Junaid, F. Munir, M. T. Waseem, S. Majeed and S. A. Shahzad, AIEE active new fluorescent and colorimetric probes for solution and vapor phase detection of nitrobenzene: A reversible mechanochromism and application of logic gate, *Microchem. J.*, 2022, **175**, 107227, DOI: **10.1016/j.microc.2022.107227**.

7 P. Yao, W. Qiao, Y. Wang, H. Peng, X. Xie and Z. a. Li, Deep-red emissive squaraine-aiegenin elastomer enabling high contrast and fast thermoresponse for anti-counterfeiting and temperature sensing, *Chem.–Eur. J.*, 2022, **28**, e202200725, DOI: **10.1002/chem.202200725**.

8 S. M. Rojas-Montoya, M. Vonlanthen, R. D. Martínez-Serrano, F. Cuétara-Guadarrama, G. Burillo and E. Rivera, New photoluminescent polyethylene films grafted with a fluoresceinderivative using gamma radiation, *Radiat. Phys. Chem.*, 2022, **194**, 110018, DOI: **10.1016/j.radphyschem.2022.110018**.

9 R. Zhao, Y. Wu, Y. Zhang, J. Ling, X. Liu, J. Xiang, X. Zeng and T. Chen, Designinganticancer combretastatin A-4 analogues with aggregation-induced emissioncharacteristics, *Sci. China: Chem.*, 2022, 1–5, DOI: **10.1007/s11426-021-1197-4**.

10 D.-D. Wang, J. Zhang, Q.-Q. Yu, K. Zhang, T.-T. Chen and X. Chu, Biomineralized zeoliticimidazolate framework-8 nanoparticles enable polymerase-driven DNA biocomputing for reliable cell identification, *Anal. Chem.*, 2022, 4794–4802, DOI: **10.1021/acs.analchem.1c05605**.

11 X. Han, J. Tong, G. Ding, C. Sun, X. Wang, Z. Su, J. Sun, L.-L. Wen and G.-G. Shan, Highly emissive coordination polymer derived from tetraphenylethylene-tetrazole chromophore: Synthesis, characterization and piezochromic luminescent behavior, *Chin. Chem. Lett.*, 2022, DOI: **10.1016/j.cclet.2022.02.060**.

12 P. Meti and Y.-D. Gong, Unveiling the structure-property relationship of X-shaped pyrazinebased DA type luminophores with tunable aggregation-induced emission, *J. Photochem. Photobiol., A*, 2022, 113908, DOI: **10.1016/j.jphotochem.2022.113908**.

13 K. D. Amirchand and V. Singh, Speed of sound, and surface tension of binary aqueoussolutions containing ammonium based protic ionic liquids, *J. Mol. Liq.*, 2022, 118845, DOI: **10.1016/j.molliq.2022.118845**.

14 Y. Sun, W. J. Neary, Z. P. Burke, H. Qian, L. Zhu and J. S. Moore, Mechanically triggeredcarbon monoxide release with turn-on Aggregation-Induced Emission, *J. Am. Chem. Soc.*, 2022, **144**, 1125–1129, DOI: **10.1021/jacs.1c12108**.

15 M. T. Waseem, H. M. Junaid, S. Majeed, A. M. Khan, T. Mahmood and S. A. Shahzad, Fluorenebased fluorescent and colorimetric chemosensors for selective detection of cyanide ions inaqueous medium and application of logic gate, *Microchem. J.*, 2022, **173**, 107018, DOI: **10.1016/j.microc.2021.107018**.

16 K.-S. Lee, H.-J. Kim, G.-H. Kim, I. Shin and J.-I. Hong, Fluorescent chemodosimeter for selective detection of cyanide in water, *Org. Lett.*, 2008, **10**, 49–51, DOI: **10.1021/ol7025763**.

17 M. A. Kaloo and J. Sankar, Reusable and specific proton transfer signalling by inorganic cyanide in solution and solid phase, *Chem. Commun.*, 2015, **51**, 14528–14531, DOI: **10.1039/C5CC05106A**.

18 J.-L. Fillaut, H. Akdas-Kilig, E. Dean, C. Latouche and A. Boucekkine, Switching of reverse charge transfers for a rational design of an off–on phosphorescent chemodosimeter of cyanide anions, *Inorg. Chem.*, 2013, **52**, 4890–4897, DOI: **10.1021/ic302478e**.

19 R. Sukato, N. Sangpetch, T. Palaga, S. Jantra, V. Vchirawongkwin, C. Jongwohan, M. Sukwattanasinitt and S. Wacharasindhu, New turn-on fluorescent and colorimetric probe for cyanide detection based on BODIPY-salicylaldehyde and its application in cell imaging, *J. Hazard. Mater.*, 2016, **314**, 277–285, DOI: **10.1016/j.jhazmat.2016.04.001**.

20 Z. Xu, X. Chen, H. N. Kim and J. Yoon, Sensors for the optical detection of cyanide ion, *Chem. Soc. Rev.*, 2010, **39**, 127–137, DOI: **10.1039/B907368J**.

21 X. Li, X. Gao, W. Shi and H. Ma, Design strategies for water-soluble small molecular chromogenic and fluorogenic probes, *Chem. Rev.*, 2014, **114**, 590–659, DOI: **10.1021/cr300508p**.

22 S.-T. Wang, J.-L. Chir, Y. Jhong and A.-T. Wu, A turn-on fluorescent sensor for detection of cyanide in aqueous media, *J. Lumin.*, 2015, **167**, 413–417, DOI: **10.1016/j.jlumin.2015.06.046**.

23 S. Erdemir and S. Malkondu, Visual and quantitative detection of CN- ion in aqueous media by an HBT-Br and thiazolium conjugated fluorometric and colorimetric probe: Real samples and useful applications, *Talanta*, 2021, **221**, 121639, DOI: **10.1016/j.talanta.2020.121639**.

24 S.-C. Wei, P.-H. Hsu, Y.-F. Lee, Y.-W. Lin and C.-C. Huang, Selective detection of iodide and cyanide anions using gold-nanoparticle-based fluorescent probe, *ACS Appl. Mater. Interfaces*, 2012, **4**, 2652–2658, DOI: **10.1021/am3003044**.

25 X. Lou, L. Qiang, J. Qin and Z. Li, A new rhodamine-based colorimetric cyanide chemosensor: convenient detecting procedure and high sensitivity and selectivity, *ACS Appl. Mater. Interfaces*, 2009, **1**, 2529–2535, DOI: **10.1021/am900467b**.

26 D. Aydin, Sensing of aluminum and cyanide ions utilizing a novel bis-phenol a based fluorogenic probe: Applications in test strips, *Microchem. J.*, 2020, **159**, 105477, DOI: **10.1016/j.microc.2020.105477**.

27 Z. Guo, Q. Niu, Q. Yang, T. Li and H. Chi, A highly selective and sensitive dual-mode sensor for colorimetric and turn-on fluorescent detection of cyanide in water, agro-products and living cells, *Anal. Chim. Acta*, 2019, **1065**, 113–123, DOI: **10.1016/j.aca.2019.03.024**.

28 S. Cheng, X. Pan, M. Shi, T. Su, C. Zhang, W. Zhao and W. Dong, A coumarin-connected carboxylic indolinium sensor for cyanide detection in absolute aqueous medium and its application in biological cell imaging, *Spectrochim. Acta, Part A*, 2020, **228**, 117710, DOI: **10.1016/j.saa.2019.117710**.

29 M. T. Waseem, H. M. Junaid, H. Gul, Z. A. Khan, C. Yu and S. A. Shahzad, Fluorene based fluorescent and colorimetric sensors for ultrasensitive detection of nitroaromatics in aqueous medium, *J. Photochem. Photobiol., A*, 2022, **425**, 113660, DOI: **10.1016/j.jphotochem.2021.113660**.

30 R. Batool, N. Riaz, H. M. Junaid, M. T. Waseem, Z. A. Khan, S. Nawazish, U. Farooq, C. Yu and S. A. Shahzad, Fluorene-based fluorometric and colorimetric conjugated polymers for sensitive detection of 2,4,6-trinitrophenol explosive in aqueous medium, *ACS Omega*, 2022, 7(1), 1057–1070, DOI: **10.1021/acsomega.1c05644**.

31 H. M. Junaid, M. T. Waseem, Z. A. Khan, H. Gul, C. Yu, A. J. Shaikh and S. A. Shahzad, Fluorescent and colorimetric sensors for selective detection of TNT and TNP explosives in aqueous medium through fluorescence emission enhancement mechanism, *J. Photochem. Photobiol., A*, 2022, **428**, 113865, DOI: **10.1016/j.jphotochem.2022.113865**.

32 Q. Ilyas, M. T. Waseem, H. M. Junaid, Z. A. Khan, F. Munir, A. J. Shaikh and S. A. Shahzad, Fluorescein based fluorescent and colorimetric sensors for sensitive detection of TNP

explosive in aqueous medium: Application of logic gate, *Spectrochim. Acta, Part A*, 2022, **272**, 120994, DOI: **10.1016/j.saa.2022.120994**.

33 S. Hussain, H. M. Junaid, M. T. Waseem, W. Rauf, A. J. Shaikh and S. A. Shahzad, Aggregation-Induced Emission of Quinoline Based Fluorescent and Colorimetric Sensors for Rapid Detection of Fe^{3+} and 4-Nitrophenol in Aqueous Medium, *Spectrochim. Acta, Part A*, 2022, **272**, 121021, DOI: **10.1016/j.saa.2022.121021**.

34 H. M. Junaid, M. T. Waseem, Z. A. Khan, F. Munir, S. Sohail, U. Farooq and S. A. Shahzad, Fluorenone-Based Fluorescent and Colorimetric Sensors for Selective Detection of I⁻ Ions: Applications in HeLa Cell Imaging and Logic Gate, *ACS Omega*, 2022, **11**, 9730–9742, DOI: **10.1021/acsomega.1c07279**.

35 F. Munir, M. T. Waseem, Z. A. Khan, S. Majeed, U. Farooq and S. A. Shahzad, Synthesis of AIEE active triazine based new fluorescent and colorimetric probes: A reversible mechanochromism and sequential detection of picric acid and ciprofloxacin, *J. Photochem. Photobiol., A*, 2022, **429**, 113921, DOI: **10.1016/j.jphotochem.2022.113921**.

36 S. Majeed, H. M. Junaid, M. T. Waseem, T. Mahmood, U. Farooq and S. A. Shahzad, Receptor free fluorescent and colorimetric sensors for solution and vapor phase detection of hazardous pollutant nitrobenzene; a new structural approach to design AIEE active and piezofluorochromic sensors, *J. Photochem. Photobiol., A*, 2022, **431**, 114022, DOI: **10.1016/j.jphotochem.2022.114022**.

37 S. Majeed, H. M. Junaid, M. T. Waseem, Z. A. Khan, A. M. Khan and S. A. Shahzad, Mechanochromic and AIE active fluorescent probes for solution and vaporphase detection of picric acid: Application of logic gate, *J. Photochem. Photobiol., A*, 2022, **432**, 114057, DOI: **10.1016/j.jphotochem.2022.114057**.

38 S. Majeed, T. A. Khan, M. T. Waseem, H. M. Junaid, A. M. Khan and S. A. Shahzad, A ratiometric fluorescent, colorimetric, and paper sensor for sequentialdetection of Cu2+ and glutathione in food: AIEE and reversible piezofluorochromic activity, *J. Photochem. Photobiol., A*, 2022, **431**, 114062, DOI: **10.1016/j.jphotochem.2022.114062**.

39 M. Haidekker, T. Brady, D. Lichlyter and E. Theodorakis, Effects of solvent polarity and solvent viscosity on the fluorescent properties of molecular rotors and related probes, *Bioorg. Chem.*, 2005, **33**, 415–425, DOI: **10.1016/j.bioorg.2005.07.005**.

40 Y. Zhang, D. Li, Y. Li and J. Yu, Solvatochromic AIE luminogens as supersensitive water detectors in organic solvents and highly efficient cyanide chemosensors in water, *Chem. Sci.*, 2014, **5**, 2710–2716, DOI: **10.1039/C4SC00721B**.

41 S. K. Burla and S. P. Pinnelli, Enrichment of gas storage in clathrate hydrates by optimizing the molar liquid water–gas ratio, *RSC Adv.*, 2022, **12**, 2074–2082, DOI: **10.1039/D1RA07585C**.

42 K. Keshav, P. Torawane, M. K. Kumawat, K. Tayade, S. K. Sahoo, R. Srivastava and A. Kuwar, Highly selective optical and reversible dual-path chemosensor for cyanide

43 M. T. Waseem, H. M. Junaid, S. Majeed, A. M. Khan, T. Mahmood and S. A. Shahzad, Fluorenebased fluorescent and colorimetric chemosensors for selective detection of cyanide ions inaqueous medium and application of logic gate, *Microchem. J.*, 2021, **173**, 107018, DOI: **10.1016/j.microc.2021.107018**.

44 W. H. Organization, *Guidelines for drinking-water quality*, World Health Organization, 1993.

45 M. Frisch, G. Trucks, H. B. Schlegel, G. E. Scuseria, M. A. Robb, J. R. Cheeseman, G. Scalmani, V. Barone, B. Mennucci and G. Petersson, *Gaussian*, Gaussian, Inc., Wallingford CT, 2009, 201.

46 A. E. Aliev, D. Courtier-Murias and S. Zhou, Scaling factors for carbon NMR chemical shifts obtained from DFT B3LYP calculations, *J. Mol. Struct.: THEOCHEM*, 2009, **893**, 1–5, DOI: **10.1016/j.theochem.2008.09.021**.

47 A. Frisch, *Gaussian 09W Reference*, Wallingford, USA, 2009, p. 25.

48 M. Asif, H. Sajid, K. Ayub, M. Ans and T. Mahmood, A first principles study on electrochemical sensing of highly toxic pesticides by using porous C_4N nanoflake, *J. Phys. Chem. Solids*, 2022, **160**, 110345, DOI: **10.1016/j.jpcs.2021.110345**.

49 M. Asif, H. Sajid, K. Ayub, A. A. Khan, R. Ahmad, M. Ans and T. Mahmood, Nano-porous C4N as a toxic pesticide's scavenger: A quantum chemical approach, *J. Mol. Graphics Modell.*, 2022, **111**, 108078, DOI: **10.1016/j.jmgm.2021.108078**.

50 N. Kosar, H. Tahir, K. Ayub, M. A. Gilani, M. Imran and T. Mahmood, Remarkable nonlinear optical response of $Mn@C_{20}$ (M = Na & K and n = 1–6); a DFT outcome, *Mater. Sci. Semicond. Process.*, 2022, **138**, 106269, DOI: **10.1016/j.mssp.2021.106269**.

51 S.-H. Jang, S.-G. Kim, D.-H. Jung, H.-J. Kwon, J.-W. Song, S.-D. Cho, Y.-C. Ko and H.-L. Sohn, Aggregation-induced emission enhancement of polysilole nanoaggregates, *Bull. Korean Chem. Soc.*, 2006, **27**, 1965–1966, DOI: **10.5012/bkcs.2006.27.12.1965**.

52 Z. Ning, Z. Chen, Q. Zhang, Y. Yan, S. Qian, Y. Cao and H. Tian, Aggregation-inducedemission (AIE)-active starburst triarylamine fluorophores as potential non-doped red 32 emitters for organic light-emitting diodes and Cl2 gas chemodosimeter, *Adv. Funct. Mater.*, 2007, **17**, 3799–3807, DOI: **10.1002/adfm.200700649**.

53 R. R. Dash, A. Gaur and C. Balomajumder, Cyanide in industrial wastewaters and its removal: a review on biotreatment, *J. Hazard. Mater.*, 2009, **163**, 1–11, DOI: **10.1016/j.jhazmat.2008.06.051**.

54 P. S. Kumar, P. R. Lakshmi and K. P. Elango, An easy to make chemoreceptor for the selective ratiometric fluorescent detection of cyanide in aqueous solution and in food materials, *New J. Chem.*, 2019, **43**, 675–680, DOI: **10.1039/C8NJ05587D**.

55 X. Lou, Y. Zhang, Q. Li, J. Qin and Z. Li, A highly specific rhodamine-based colorimetric probe for hypochlorites: A

detection and its application in live cells imaging, *Biosens. Bioelectron.*, 2017, **92**, 95–100, DOI: **10.1016/j.bios.2017.02.006**.

new sensing strategy and real application in tap water, *Chem. Commun.*, 2011, **47**, 3189–3191, DOI: **10.1039/C0CC04911E**.

56 X. Cheng, Y. Zhou, J. Qin and Z. Li, Reaction-based colorimetric cyanide chemosensors: Rapid naked-eye detection and high selectivity, *ACS Appl. Mater. Interfaces*, 2012, **4**, 2133–2138, DOI: **10.1021/am3001083**.

57 M. Orojloo and S. Amani, Naked-eye detection of cyanide ions in aqueous media based on anazo-azomethine chemosensor, *C. R. Chim.*, 2017, **20**, 415–423, DOI: **10.1016/j.crci.2016.07.003**.

58 H. Muniyasamy, C. Chinnadurai, M. Nelson, A. M. Kubendran, K. Sukumaran, A. Balasubramaniem, M. Sepperumal, S. Ayyanar, M. Govindasamy and A. Ghfar,

Highly selective flurogenic chemosensor for cyanide ion in aqueous medium and its applications of logic gate and HeLa cells, *J. Mol. Liq.*, 2021, **334**, 116076, DOI: **10.1016/j.molliq.2021.116076**.

59 A. Ozdemir and S. Erdemir, Phenanthroimidazole and dicyanovinyl-substituted triphenylamine for the selective detection of CN-: DFT calculations and practically applications, *J. Photochem. Photobiol., A*, 2020, **390**, 112328, DOI: **10.1016/j.jphotochem.2019.112328**.

60 K. Szaciłowski, Digital Information Processing in Molecular Systems, *Chem. Rev.*, 2008, **108**, 3481–3548, DOI: **10.1021/cr068403q**.